Dyes and Pigments 95 (2012) 723–731

Contents lists available at SciVerse ScienceDirect

Dyes and Pigments

journal homepage: www.elsevier.com/locate/dyepig

New five-coordinated mercury (II) dyes based on a novel 2,2′:6′,2″-terpyridine ligand: Structures, photophysical properties and DFT calculations to evaluate the halogen effect on the two-photon absorption

Hongping Zhou [a,*], Jianqing Wang [a], Feixia Zhou [a], Dongling Xu [a], Yuanle Cao [a], Gang Liu [a], Lin Kong [a], Jiaxiang Yang [a], Jieying Wu [a], Yupeng Tian [a,b,c]

[a] College of Chemistry and Chemical Engineering, Anhui University and Key Laboratory of Functional Inorganic Materials Chemistry of Anhui Province, 230039 Hefei, PR China
[b] State Key Laboratory of Crystal Materials, Shandong University, 250100 Jinan, PR China
[c] State Key Laboratory of Coordination Chemistry, Nanjing University, 210093 Nanjing, PR China

ARTICLE INFO

Article history:
Received 30 April 2012
Received in revised form
4 July 2012
Accepted 4 July 2012
Available online 13 July 2012

Keywords:
Five-coordinated mercury (II)
Single crystal
Linear optical properties
Nonlinear optical properties
DFT calculations
TPA cross-sections

ABSTRACT

A simple D-π-A type ligand (**L**: 4′-(4-[4-(1H-[1,2,4]-triazolyl)styryl]phenyl)-2,2′:6′,2″-terpyridine) was designed and synthesized, which reacted with HgX_2 (X = Cl, Br, I, SCN) yielding a series of uncommon five-coordinated mercury (II) complexes (**Dyes 1**–**4**). The ligand and **Dye 4** were characterized by single crystal X-ray diffraction determination. Linear and nonlinear optical properties of the ligand and dyes were exhibited. Experimental results revealed that the two-photon absorption (TPA) cross-sections of the four dyes are considerably larger than that of the ligand. Density function theory (DFT) calculations performed on **Dyes 1**–**4** showed that the halogens affect the accepting capability of the complexed metal due to different electron inductive effects, which finally influence the TPA cross-section values.

1. Introduction

Two-photon absorption (TPA) is a three-order nonlinear optical process and offers various advantages, including localized excitation at the focal point of the objective and minimal photochemical damage. Materials with large two-photon absorption cross-section are in great demand for a variety of applications, including 3D microfabrication [1], two-photon excited fluorescence microscopy [2], optical power limiting [3], and photodynamic therapy [4].

It is well established that TPA cross-sections depend critically on the strength of the chromophore's two-photon absorptivity. To date, many molecules with a larger TPA cross-section (δ_{TPA}) have been widely investigated *via* two main approaches. One is to design complex structures mainly based on the intra-molecular interaction, such as donor–bridge–acceptor (D–π–A) dipoles, donor–bridge–donor (D–π–D) quadrupoles, multibranched compounds, dendrimers, octupoles, and porphyrins [5]. These study results reveal that TPA cross-sections increase with the donor/acceptor strength, conjugation length, and planarity of the π-center. The other is defined as inter-molecular interaction starting from simple molecular units organized in supramolecular self-assembled structures [6]. Such research indicates that the existing weak interactions may induce rearrangement of electrons and optimized orientation of compounds to enhance TPA cross-section.

In the current work, first, terpyridine was selected as the A (acceptor) group, because it possesses two important aspects that make it an ideal building block for fluorescent molecular materials [7]: (i) a superb ability to coordinate with different metal ions (ii) a rigid framework plane, which leads generally to form a larger planar systems. Second, the enolic styrene acts as π-conjugated unit, which can lead to a higher degree of π-electron delocalization [8]. Finally, electron-rich triazole works as the D (donor) group and coordination group (Fig. 1).

Synthetic strategy was based on the molecular self-assembly of organic ligand with TPA properties and different inorganic salts to product materials with larger δ_{TPA}. A series of new coordination complexes (**Dyes 1**–**4**) with five-coordinated mercury (II) were

---

* Corresponding author. Tel.: +86 5515108151; fax: +86 5515107342.
E-mail address: zhpzhp@263.net (H. Zhou).

0143-7208/$ – see front matter © 2012 Published by Elsevier Ltd.
http://dx.doi.org/10.1016/j.dyepig.2012.07.005

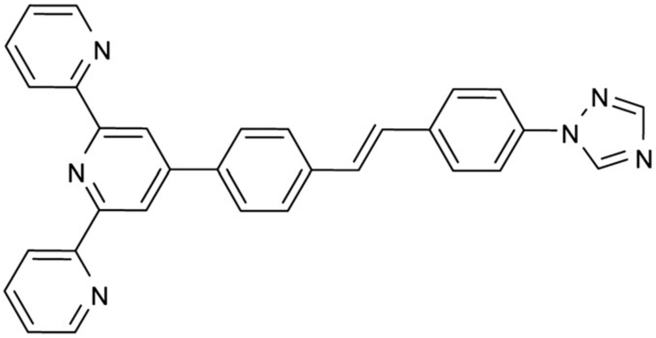

Fig. 1. Structure of the ligand (**L**).

obtained by self-assembling the ligand with HgX_2 (X = Cl, Br, I, SCN). **L** and **Dye 4** were characterized by single crystal X-ray diffraction determination. Linear and nonlinear optical properties of the ligand and four dyes were investigated.

2. Experimental section

2.1. Materials and physical measurements

UV–vis absorption spectra were recorded on a UV-3100 spectrophotometer. Fluorescence measurements were carried out using an Edinburgh FLS920 fluorescence spectrometer equipped with a 450 W Xe lamp and a time-correlated single-photon counting (TCSPC) card. All the fluorescence spectra were collected. The single-photon excited fluorescence (SPEF) quantum yields (Φ) were measured by using a standard method under the same experimental conditions for all compounds. Rhodamine B dissolved in ethanol ($\Phi = 0.56$) [9] at the same concentration as the other samples was used as the standard. The two-photon excited fluorescence (TPEF) spectra were measured using a Mira 900-D Ti: sapphire femtosecond laser with a pulsewidth of 200 fs and a repetition rate of 76 MHz. All measurements were carried out in air at room temperature. TPA cross-sections were measured using fluorescein as reference.

2.2. Materials and synthesis

All chemicals were available commercially from Acros Organics company (Beijing) and Aladdin (Shanghai), and the solvents were purified via conventional methods before use. IR spectra were recorded with a Nicolet FT-IR NEXUS 870 spectrometer (KBr discs) in the 4000–400 cm^{-1} region. ^1H NMR and ^{13}C NMR spectra were recorded on a 400 MHz NMR instrument using $CDCl_3$ as solvents. Mass spectra were obtained on a Micromass GCT-MS Spectrometer. Elemental analysis was recorded on Perkin Elmer 240B instrument.

2.2.1. Preparation of the ligand: (4′-(4-[4-(1H-[1,2,4]-triazolyl) styryl] phenyl)-2,2′:6′,2″-terpyridine)

The ligand was readily achieved in 78.1% yield by Solid-state Wittig reaction with 4-(2,2′:6′,2″-terpyridine-4′-yl)-benzyltriphenylphosphonium bromide [10] and 4-(1H-[1,2,4]-triazol-1-yl) benzaldehyde [11]. ^1H NMR ($CDCl_3$, 400 MHz): 7.47 (s, 2H), 7.53–7.56 (m, 2H), 7.85–7.87 (m, 4H), 7.92 (d, $J = 8.0$ Hz, 2H), 8.00 (d, $J = 8.0$ Hz, 2H), 8.06 (t, $J = 8.0$ Hz, 2H), 8.26 (s, 1H), 8.69 9 (d, $J = 8.0$ Hz, 2H), 8.77–8.79 (m, 4H), 9.35 (s, 1H). Ms: m/z (%) = 478.19 (100). FT-IR (KBr, cm^{-1}): 3427 (w), 3054 (w), 1583 (s), 1564 (m), 1522 (s), 1466 (m), 1388 (s), 1277 (w), 1147 (m), 965 (m), 839 (m), 789 (s), 671 (m), 537 (m). Calcd for $C_{31}H_{22}N_6$: C, 77.79; H, 4.63; N, 17.58%. Found: C, 77.57; H, 4.92; N, 17.51%.

2.2.2. Preparation of **Dyes 1–4**

L (23.9 mg, 0.05 mmol) in 15 mL of $CHCl_3$ was added into a 50 mL colorimeter tube, layered with 10 mL of ethanol (or methanol), and then HgX_2 (X = Cl, Br, I for SCN) (0.05 mmol) in 15 mL of ethanol (or methanol) was added. The solution was left for slow evaporation and crystals were collected for each case after two weeks.

*2.2.2.1. $HgLCl_2$ (**Dye 1**).* Yield: 26 mg (69%). FT-IR (KBr, cm^{-1}): 3442 (m), 3097 (w), 1595 (vs), 1572 (m), 1521 (vs), 1474 (s), 1428 (m), 1403 (m), 1278 (m), 1248 (m), 1218 (m), 1011 (m), 980 (m), 839 (m), 790 (m), 745 (m). Calcd for $C_{31}H_{22}Cl_2N_6Hg$: C, 49.64; H, 2.96; N, 11.20%. Found: C, 49.81; H, 2.99; N, 11.14%. From the calculated analysis result, we can infer the unit of **Dye 1** may contain one $HgLCl_2$.

*2.2.2.2. $[HgLBr_2]_2\cdot CHCl_3$ (**Dye 2**).* Yield: 31 mg (74%). FT-IR (KBr, cm^{-1}): 3441 (m), 3098 (w), 1594 (vs), 1571 (m), 1519 (s), 1473 (s), 1428 (m), 1402 (m), 1278 (w), 1247 (w), 1216 (w), 1009 (m), 979 (m), 838 (m), 788 (m), 742 (m). Calcd for $C_{63}H_{45}N_{12}Br_4Cl_3$ Hg_2: C, 42.10; H, 2.52; N, 9.35%. Found: C, 42.31; H, 2.57; N, 9.34%. From the calculated analysis result, we can infer the unit of **Dye 2** may contain two $HgLBr_2$ and a chloroform molecule.

*2.2.2.3. $[HgLI_2]_2\cdot CHCl_3$ (**Dye 3**).* Yield: 35 mg (75%). FT-IR (KBr, cm^{-1}): 3442 (m), 3104 (w), 1595 (vs), 1539 (m), 1521 (s), 1474 (s), 1426 (m), 1402 (m), 1278 (m), 1248 (m), 1216 (m), 1009 (m), 978 (m), 837 (m), 788 (m), 733 (m). Calcd for $C_{63}H_{45}N_{12}Cl_3I_4Hg_2$: C, 38.11; H, 2.28; N, 8.47%. Found: C, 38.29; H, 2.33; N, 8.42%. From the calculated analysis result, we can infer the unit of **Dye 3** may contain two $HgLI_2$ and a chloroform molecule.

*2.2.2.4. $HgL(SCN)_2$ (**Dye 4**).* Yield: 26 mg (65%). FT-IR (KBr, cm^{-1}): 3429 (m), 3106 (w), 2922(w), 2112 (s), 1594 (vs), 1572 (m), 1521 (s), 1474 (s), 1404 (s), 1278 (m), 1247 (m), 1214 (m), 1145 (m), 1050 (m), 1011 (m), 977 (m), 839 (m), 790 (m). Anal. Calcd for $C_{33}H_{22}N_8S_2Hg$: C, 49.84; H, 2.79; N, 14.09%. Found: C, 49.66; H, 2.64; N, 14.15%。

2.3. X-ray crystallography

Data for single crystals were collected on a Siemens Smart 1000 CCD diffractometer. The determination of unit cell parameters and data collections were performed with Mo Kα radiation ($\lambda = 0.71073$ Å). Unit cell dimensions were obtained with least-squares refinements, and all structures were solved by direct methods using SHELXS-97 [12]. The other non-hydrogen atoms were located in successive difference Fourier syntheses. The final refinement was performed by using full-matrix least-squares methods with anisotropic thermal parameters for non-hydrogen atoms on F^2. The hydrogen atoms were added theoretically and processing parameters for **Dye 4** and **L** are shown in Table 1 and the selected bond lengths and bond angles are listed in Table 2.

3. Results and discussion

L crystallized in the monoclinic form with the space group $P2_{(1)}/C$ as shown in Fig. 2(a). The unit contains two molecules. In each molecule, the dihedral angel between the terpyridine ring and its bonded benzene ring is 10.841°, showing a distorted plane.

Single crystal X-ray structural analysis shows that the asymmetric unit of **Dye 4** consists of one Hg(II), one **L**, two thiocyanate anions (Fig. 3(a)). The Hg (II) center is five-coordinated by three nitrogen atoms from one **L** and two sulfur atoms from two thiocyanate anions. The bond lengths Hg1–N1, Hg1–N2, Hg1–N3 are 2.417(9), 2.367(8), 2.39(1) Å respectively. Each bond angle around

Table 1
Crystallographic data for **L** and **Dye 4**.

Compound	HgL(SCN)$_2$	L
Empirical formula	$C_{33}H_{22}N_8S_2Hg$	$C_{31}H_{22}N_6$
Formula weight	795.30	478.55
Crystal system	Monoclinic	Monoclinic
Space group	C2/c	$P2_{(1)}/C$
a [Å]	13.806(5)	9.513(19)
b [Å]	25.080(5)	46.843(9)
c [Å]	18.629(5)	11.521(2)
β [°]	102.360(5)	113.441(3)
V [Å^3]	6301(3)	4710.3(16)
Z	8	8
T [K]	298(2)	298(2)
D_{calcd} [g cm^{-3}]	1.677	1.350
μ [mm^{-1}]	5.055	0.083
θ range [°]	1.71–25.00	0.87–25
Total no. data	5556	8292
No. unique data	3314	3111
No. parameters refined	397	667
R_1	0.0564	0.0623
wR_2	0.1905	0.1377
GOF	1.107	0.915

the mercury atom is in the range 67.9(3)–137.5(2)°, indicating a quite distorted tetrahedral geometry.

The data analysis demonstrated the dihedral angel between the terpyridyl ring and its bonded benzene ring is only 3.06°, smaller than that of **L**. The alkene π-bridge unit is basally co-planar with each phenyl ring, because the linkage bond lengths between benzene rings and alkene π-bridge unit are quiet conjugated, C18–C21 [1.450(15)], C21–C22 [1.304(15)], C22–C23 [1.483(14)]. On the other hand, the alkene π-bridge unit exhibits enolic structure. These structure features of **Dye 4** suggested that all non-hydrogen atoms of the unit are highly conjugated, leading to a π-bridge for charge transfer, which may enlarge the molecular TPA cross-section [5a].

Table 2
Selected bond lengths (Å) and angles (°) for **L** and **Dye 4**.

L			
N1–C47	1.346(6)	N10–N11	1.348(6)
N1–C49	1.343(6)	N10–C4	1.324(6)
N2–C52	1.336(7)	N11–C1	1.310(7)
N2–C56	1.346(8)	N12–C1	1.334(7)
N3–C38	1.319(8)	N12–C4	1.320(7)
N3–C42	1.326(7)	C47–N1–C49	117.7(4)
N4–C22	1.339(6)	C52–N2–C56	116.2(4)
N4–C24	1.338(6)	C38–N3–C42	118.4(5)
N5–C32	1.334(8)	C22–N4–C24	117.3(4)
N5–C35	1.330(7)	C32–N5–C35	117.3(4)
N6–C26	1.340(7)	C26–N6–C30	117.3(4)
N6–C30	1.335(8)	C75–N7–N8	108.3(4)
N7–N8	1.361(7)	C74–N8–N7	102.9(4)
N7–C75	1.341(7)	C74–N9–C75	102.6(5)
N8–C74	1.321(7)	C4–N10–N11	108.2(4)
N9–C74	1.341(9)	C1–N11–N10	102.8(4)
N9–C75	1.318(6)	C1–N12–C2	101.4(4)
HgL(SCN)$_2$			
Hg1–N1	2.417(9)	N1–Hg1–N3	136.1(3)
Hg1–N2	2.367(8)	S1–Hg1–S2	114.01(14)
Hg1–N3	2.39(1)	S1–Hg1–N1	98.4(3)
Hg1–S1	2.540(4)	S1–Hg1–N2	107.9(2)
Hg1–S2	2.451(4)	S1–Hg1–N3	100.6(2)
S1–C33	1.63(2)	S2–Hg1–N1	98.7(2)
S2–C30	1.55(1)	S2–Hg1–N2	137.5(2)
N6–C30	1.16(2)	S2–Hg1–N3	108.9(2)
N8–C33	1.13(1)	S1–C33–N8	176.1(15)
N1–Hg1–N2	67.9(3)	S2–C30–N6	175.4(16)

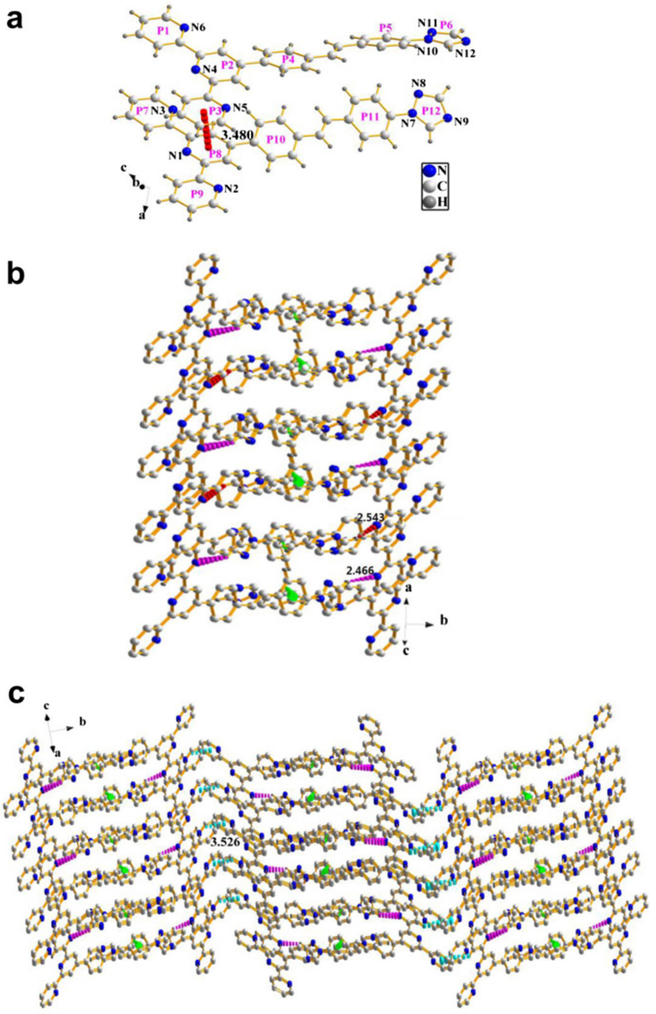

Fig. 2. (a) Single crystal structure of L. (b) The 1-D framework of L showing the C–H···N (purple and red) hydrogen bond and C–H···π interaction (light green) along the c-axis. (c) The 2-D framework of L showing C–H···π interaction along the b-axis. (For interpretation of the references to colour in this figure legend, the reader is referred to the web version of this article.)

In addition, **L** generated a 1-D chain through C–H···N (purple dashed line 2.466 Å, red dashed line 2.543 Å) and C–H···π contacts (light green dashed line 3.197 Å, for interpretation of the references to colour in this figure, the reader is referred to the web version of this article) (Fig. 2(b)). Further more C–H···π contacts (blue dashed line 3.526 Å) resulted in a 2-D framework (Fig. 2(c)). **Dye 4** formed its 1-D chain *via* C–H···S (light green dashed line 2.974 Å) and π–π stacking contacts (red dashed line), the shortest distance is 3.352 Å (Fig. 3(b), for interpretation of the references to colour in this figure, the reader is referred to the web version of this article). Its 2-D structure was obtained when the C–H···N (purple dashed line 2.538 Å) interaction pulled chains together (Fig. 3(c)). Further more, the adjacent interpenetrating layers are held together by C–H···S (red dashed line 2.938 Å, blackish green dashed line 2.865 Å) interactions to afford an extended 3-D supramolecular framework (Fig. 3(d)). Structures with different geometries between **L** and **Dye 4** may be vital factors affecting δ_{TPA}. Supramolecular self-assembled structures brought size-enhanced nonlinearities which formed an extremely concentrated fluorophore, cooperatively enhancing δ_{TPA} [6].

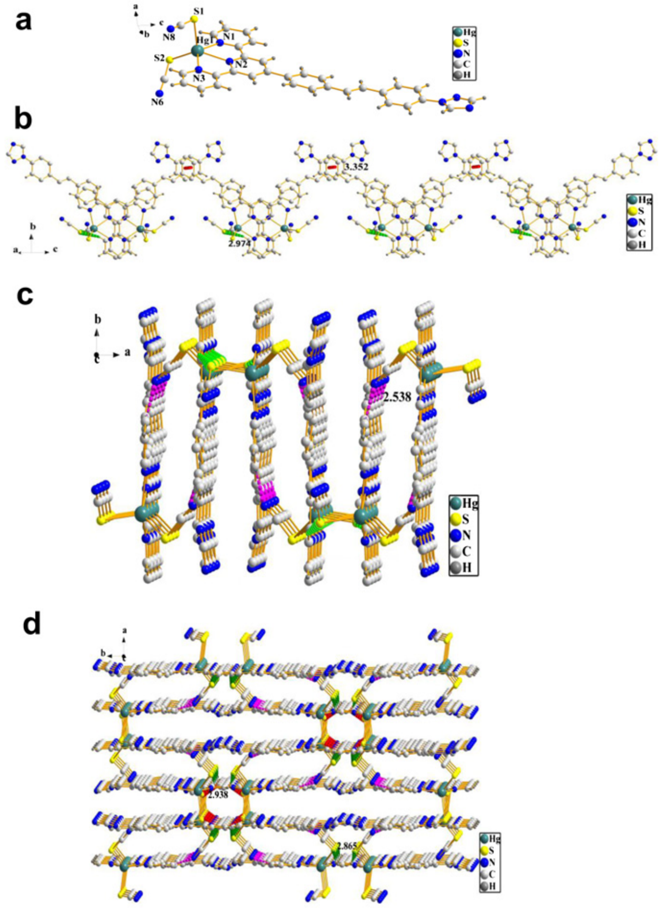

Fig. 3. (a) Coordination environments of Hg with the atom numbering scheme. (b) The 1-D framework of **Dye 4** showing the C–H···S (light green) hydrogen bond and π–π stacking (red) along the *c*-axis. (c) The 2-D framework of **Dye 4** showing C–H···N (purple) hydrogen bond along the *a*-axis. (d) The 3-D architecture of **Dye 4** showing the C–H···S (blackish green) hydrogen bond along the *b*-axis. (For interpretation of the references to colour in this figure legend, the reader is referred to the web version of this article.)

4. Theoretical calculation

4.1. Calculation details

The structures were optimized by using the density-functional theory with the 6–31G(d) basis set for the C, H, O, S atoms and with the LANL2DZ basis set for the Hg, Br, I atoms [13]. DFT calculations were carried out using B3LYP (Becke's three-parameter hybrid exchange-correlation (x-c) functional) [14]. All the geometry optimizations were carried out with no symmetry constraint. Excitation energy calculations were carried out using TDDFT [15], as implemented in the Gaussian 03 programs [16].

The structure–property relationships for the various design approaches have been extensively reviewed [17]. For noncentresymmetric dipolar fluorophores, the attachment of an electron-rich donor and an electron deficient acceptor group to a linear π-system typically results in an uneven, dipolar ground state charge distribution. Upon photoexcitation, such dipolar fluorophores undergo charge redistribution from the donor to the acceptor group to give a further polarized excited state with an increased dipole moment compared to the ground state. Applying a simplified two-state model that only includes the electronic ground state S_0 and the lowest excited state S_1, the peak cross-section $\delta_{\max}$ at the two-photon resonance energy ($2h\nu = E_1$) is related to the transition dipole moment M_{01} and the change in permanent dipole moment $\Delta\mu = \mu_{01} - \mu_0$ between ground and excited state according to Eq. [18].

$$\delta_{\max} = \frac{2\pi L^4}{5 s_0^2 n^2 c^2 h} \frac{(\Delta\mu)^2 M_{01}^2}{\Gamma} \tag{1}$$

Table 3
The results of DFT calculation, the values of E_{0f}, M_{01}, $\Delta\mu$.

Formula	E_{0f} (ev)	M_{01} (D)	$\Delta\mu$ (D)
	3.10	13.31	21.11
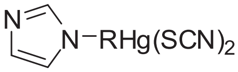	3.11	13.12	21.13
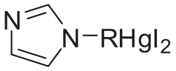	3.11	12.18	21.14
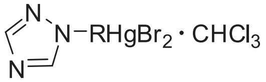	3.12	13.18	20.12
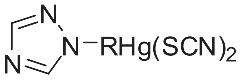	3.12	13.13	20.12
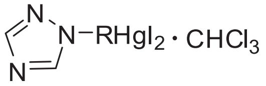	3.12	13.01	20.14

Table 4
Photophysical properties of **L**, **Dye 1**, **Dye 2**, **Dye 3**, **Dye 4** in different polar solvents.

Compd	Solvents	λ/nm[a]	λ/nm[b]	Φ[c]	$\Delta\nu$/cm^{-1}[d]
L	THF	286, 336	408	0.468963	5252
	Ethyl acetate	279, 327	404	0.549127	5829
	Ethanol	288, 332	515	0.335037	10703
	Acetonitrile	284, 330	412	0.334894	6031
	DMF	283, 333	420	0.496245	6221
	Methanol	285, 336	424	0.13953	6177
$HgCl_2$	THF	282, 335	408	0.44791	5341
	Ethyl acetate	279, 326	404	0.456052	5922
	Ethanol	290, 336	413	0.716585	5549
	Acetonitrile	281, 331	412	0.38188	5940
	DMF	286, 335	420	0.570439	6041
	Methanol	285, 331	425	0.23397	6682
$HgBr_2$	THF	284, 335	408	0.411701	5341
	Ethyl acetate	290, 322	404	0.039167	6303
	Ethanol	285, 336	414	0.613287	5607
	Acetonitrile	283, 329	412	0.436395	6123
	DMF	290, 339	420	0.489241	5689
	Methanol	282, 334	424	0.265594	6355
HgI_2	THF	284, 333	407	0.475053	5460
	Ethyl acetate	282, 324	405	0.362004	6173
	Ethanol	284, 332	415	0.564316	6024
	Acetonitrile	283, 329	414	0.421538	6241
	DMF	295, 335	419	0.58198	5984
	Methanol	282, 334	424	0.296531	6355
$Hg(SCN)_2$	THF	281, 335	409	0.456047	5401
	Ethyl acetate	284, 323	405	0.106541	6268
	Ethanol	285, 332	415	0.5374	6024
	Acetonitrile	281, 331	413	0.397672	5998
	DMF	290, 335	420	0.519437	6041
	Methanol	284, 334	423	0.27511	6299

[a] Peak position of the longest absorption band.
[b] Peak position of SPEF, excited at the absorption maximum.
[c] Quantum yields determined by using quinine sulfate as standard.
[d] Stokes' shift in cm^{-1}.

where Γ is corresponds to a damping factor that represents the overall bandwidth of the S_0–S_1 transition.

4.2. DFT calculation

In order to understand the relationship between the maximum TPA cross-sections (δ) and the different ligands, DFT calculations were performed for all the complexes. As is established, metal coordination to the terpyridinyl group increases the tendency for charge transfer under excitation. E_{0f} is corresponding to the transition energy (E_{0f}) between the ground state (0) to the final state (f). According to Eq. (1) and the maximal E_{0f}, M_{01}, $\Delta\mu$ ($\delta_{\max}$) in Table 3, these results clearly indicate that cooperative factors from M_{01} and $\Delta\mu$ that perform the TPA effect are obtained in coordination complexes. In the table, the absorption maximum is very similar, indicating that the metal binding may affect on the intensity of the absorption rather than modify the route of absorption. Further comparison of these data implies imidazole > triazole in enhancing δ. It may be elucidated that the imidazole moieties are more liable to excited state polarization than triazole, which may indicate that TPA cross-sections of coordination compounds from a ligand with large δ are often larger than one with small δ. Considering a variety of coordination modes of $HgCl_2$, we only calculated Br^-, SCN^-, I^-. The halogen affect on the metal acceptance strength by different electron inductive effect, $Br^- > SCN^- > I^-$, which is consistent with our previous study [19].

5. Linear absorption and single-photon excited fluorescence (SPEF)

The photophysical properties (absorption and fluorescence) of the novel series of dyes in six different solvents are collected in Table 4 including fluorescence quantum yield.

5.1. Absorption properties

Linear absorption spectra of **L**, **Dye 1**, **Dye 2**, **Dye 3** and **Dye 4** in benzene, ethyl acetate, THF, ethanol, acetonitrile and DMF with a solution concentration of $c = 1.0 \times 10^{-5}\ \mathrm{mol\,L^{-1}}$ are shown in Fig. 4. From Table 4, one can observe that each of their absorption

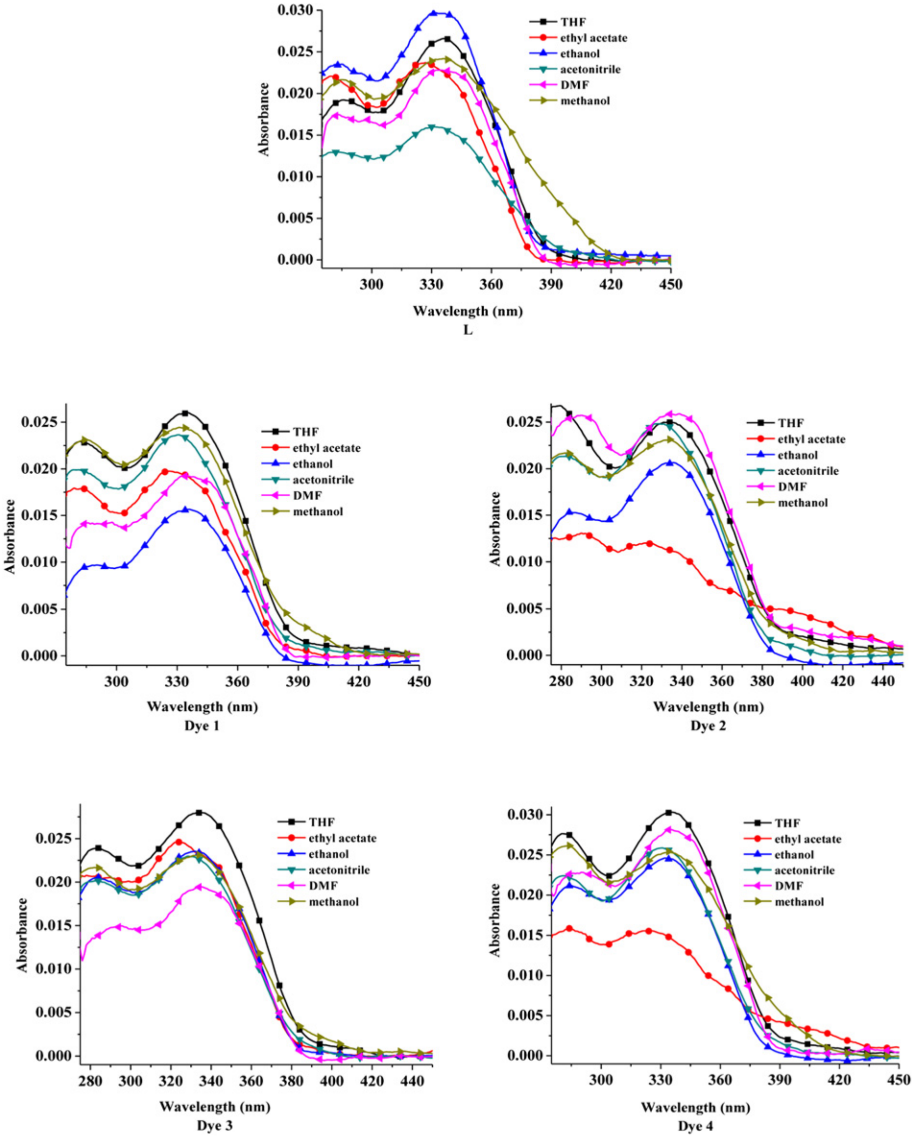

Fig. 4. Linear absorption spectra of **L**, **Dye 1**, **Dye 2**, **Dye 3** and **Dye 4** in six solvents.

spectra exhibits two peaks between 250 nm and 400 nm. The absorption maxima of **L** and four dyes are located at 333, 335, 335 and 335 nm in DMF, respectively, which corresponds to the $\pi-\pi^*$ transition of the main chain. Fig. 4 is the linear absorption spectra of **L** and four dyes in six different solvents, which shows that the peak values are not significantly different and there is no linear absorption in the entire spectral range from 450 to 900 nm.

5.2. Fluorescence properties

The SPEF spectra were measured at the same concentration as that of the linear absorption spectra. As shown in Fig. 5 and Table 4, the SPEF spectra of **L**, **Dye 1**, **Dye 2**, **Dye 3** and **Dye 4** showed slightly red shift with increase of the polarity of solvent. This can be explained by the fact that the excited state of compounds may possess higher polarity than that of the ground state, for the solvatochromism is associated with the energy level lowering [20]. Increased dipole–dipole interaction between the solute and solvent leads to lowering the energy level on some scale [21]. In addition, obvious trends of decrease in Φ occurred with increasing solvent polarity, except in DMF. These phenomena maybe caused by the non-radiative transition from the excited state to triples in different polar solvents.

Comparison of the Φ of **L** and dyes in the same solvent indicates that the dyes have higher Φ values, which is due to intra-molecular charge transfer process (ICT). After **L** was coordinated with Hg^{2+}, a larger planarity was formed and a stronger acceptor generated, possibly inducing charge delocalization on a greater scale.

5.3. Two-photon excited fluorescence (TPEF)

The two-photon excited fluorescence spectra (TPEF) of compounds **L**, **Dye 1**, **Dye 2**, **Dye 3** and **Dye 4** in DMF were recorded at different excited wavelengths. The results are shown in Fig. 5. Because there is no linear absorption in the range from 450 nm to 850 nm, the emission excited by a laser in this spectral range can be attributed to the TPEF mechanism. Fig. 6 shows a log–log plot of the excited fluorescence signal versus excited light power. It provides direct evidence for the squared dependence of excited fluorescence power and input laser intensity.

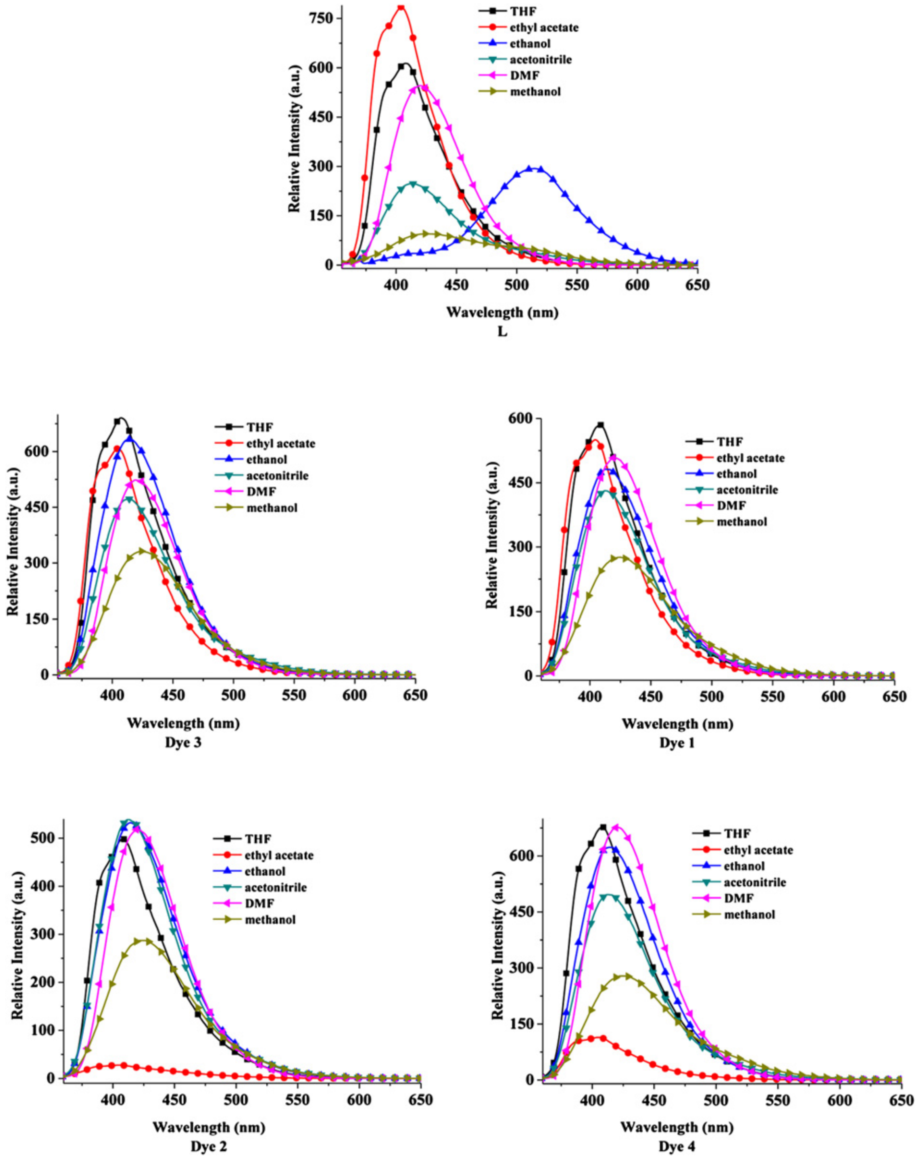

Fig. 5. The one-photon fluorescence spectra of **L**, **Dye 1**, **Dye 2**, **Dye 3** and **Dye 4**.

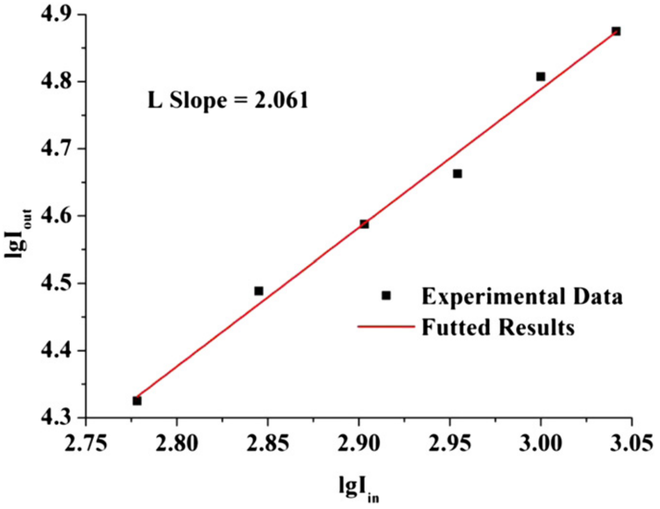

Fig. 6. Output fluorescence (I_{out}) vs. the square of input laser power (I_{in}) for **L**. Excitation was carried out at 720 nm, with $c = 1.0 \times 10^{-3}$ mol/L in DMF.

As shown in Fig. 7, the TPA spectra of **L** and **Dye 1** are determined in the wavelength range by investigating their two-photon excited fluorescence (TPEF) in DMF with a concentration of 1.0×10^{-3} mol/L. The TPA spectra of the other dyes are similar to that of **Dye 1**. The absorption maxima lengths locate at 442 and 484 nm for **L**, 526 nm for **Dye 1**, **Dye 2** and **Dye 3**, 538 nm for **Dye 4** in DMF, respectively.

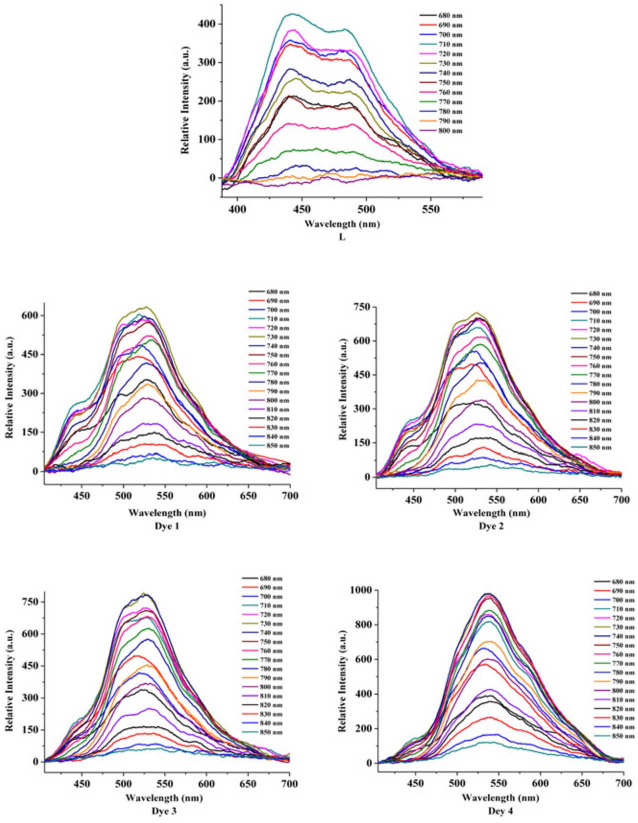

Fig. 7. The TPA spectra of **L**, **Dye 1**, **Dye 2**, **Dye 3** and **Dye 4** in DMF under different excitation wavelengths.

The TPA cross-sections (δ) are determined by comparing their TPEF to that of fluorescein in DMF, according to the following equation [22]:

$$\delta = \delta_{ref} \frac{\Phi_{ref}}{\Phi} \frac{c_{ref}}{c} \frac{n_{ref}}{n} \frac{F}{F_{ref}}$$

here, the subscript ref stands for the reference molecule. δ is the TPA cross-section value, c is the concentration of solution, n is the refractive index of the solution, F is the TPEF integral intensity of the solution emitted at the exciting wavelength, and Φ is the fluorescence quantum yield. The $\delta_{ref}\mu$ value of reference was taken from the literature [23]. Detailed experiments reveal that from 680 to 850 nm, the peak position in the TPEF spectra of these complexes is independent of the excitation wavelength, but the TPA cross-sections are dependent over this range. By tuning the pump wavelength up from 680 to 850 nm while keeping the input power fixed and then recording the TPEF intensity, the two-photon absorption spectra Fig. 7 are obtained. By referencing the TPA cross-section of fluorescein to be 19 GM (1 GM = 10^{-50} cm^{-4} s photon^{-1}) [24], the maximum two-photon absorption cross-sections of complexes are 97 GM for **L**, 144.13 GM for **Dye 1**, 194.14 GM for **Dye 2**, 160.96 GM for **Dye 3** and 212.49 GM for **Dye 4** at 720 nm in DMF. Fig. 8 shows the TPA action spectrum of **L**, **L-Hg** (II) in the 680–850 nm range. It has been found that two-photon absorption cross-sections of **L-Hg** (II) from 680 to 850 nm are always larger than that of L, which is unusual for Hg^{2+} complexes. The behavior observed here in the TPA spectra, can be attributed to the enlarged conjugation length upon Hg (II) addition **L**, a new D–π–A type compound formed, in which the terpyridyl ring is the acceptor part and a triadozolyl group is the donor. When **L** is coordinated with HgX$_2$, the Hg^{2+} becomes the acceptor, which induces a larger delocalization of the electrons. In addition, dyes with different anions around Hg (II) have different TPA cross-section values, which is due to different electron inductive effect inducing further delocalization of electrons further (Fig. 9).

In order to study the effect of anions on δ_{TPA}, we tested and calculated δ_{TPA} of the similar ligand **L**′ (4′-(4-[4-(imidazolyl)styryl] phenyl)-2,2′:6′,2″-terpyridine) and its complexes based on mercury salts [19]. The maximum two-photon absorption cross-section of **L**′ is 149 GM [19] (Fig. 9), much larger than that of **L**, which agreed with the theoretical calculation. In addition,

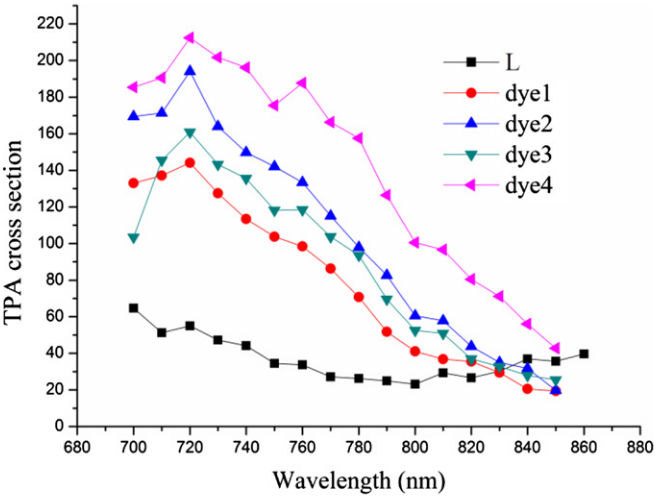

Fig. 8. Two-photon (from a 200 fs, 76 MHz, Ti: sapphire laser) absorption cross-sections of **L**, **Dye 1**, **Dye 2**, **Dye 3** and **Dye 4** in DMF versus excitation wavelengths of identical energy of 0.100 w. (experimental uncertainties: 10%).

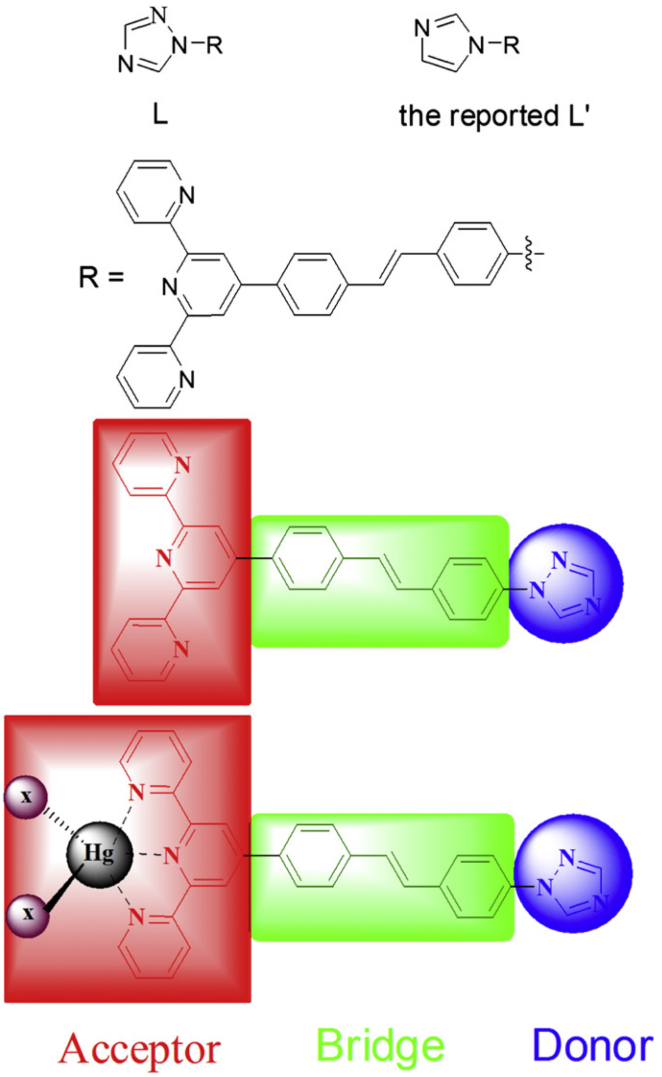

Fig. 9. D–π–A structures of **L** and its complexes.

complexes of **Hg(II)** with different anions also have different two-photon absorption cross-sections as seen from Fig. 7. Considering experimental error, the order is $I^- < Br^- < SCN^-$, which is basically consistent with theoretical results.

6. Conclusions

In summary, we have synthesized and characterized novel 2,2′:6′,2″-terpyridine-based ligand and its Hg^{2+} complexes. Single crystal structures of **L** and **Dye 4** were obtained, and supramolecular structures were investigated. Linear and nonlinear optical properties of the ligand and four dyes were exhibited. DFT calculations were performed to evaluate different anions effect on TPA cross-section values. All results further proved that better co-planar, inter-molecular interactions and anions may enhance the 2PA cross-section through cooperation effect.

Acknowledgments

This work was supported by a program for New Century Excellent Talents in university, Doctoral Program of Ministry of Education of China (20113401110004), Science and Technological Fund of An Hui Province for Outstanding Youth (10040606Y22), National Nature Science Foundation of China (21071001, 51142011, 21101001), Natural Science Foundation of Education Committee of An Hui Province (KJ 2012A024, KJ2010A030), the 211 Project of An Hui University.

Appendix A. Supplementary data

Crystallographic data reported in this paper has been deposited with the Cambridge Crystallographic Data Center, CCDC No.805571 for **L**, CCDC No.832301 for **Dye 4**. Copies of these information may be obtained free of charge from the Director, CCDC, 12 Union Road, Cambridge CB2 1EZ, UK (fax: +44 1223336033; E-mail: deposit@ccdc.cam.ac.uk). http://dx.doi.org/10.1016/j.dyepig.2012.07.005.

References

[1] (a) Zhang X, Sun YM, Yu XQ, et al. Synthesis and nonlinear optical properties of several new two-photon photopolymerization initiators about dibenzothiophene derivatives. Synthetic Metals 2009;159:2491–6;
(b) Li CW, Yang K, Feng Y, et al. Investigation of two-photon absorption induced excited state absorption in a fluorenyl-based chromophore. Journal of Physical Chemistry B 2009;113:15730–3.

[2] (a) Wang L, Tao XT, Shi JH, et al. Conjugated chromophore near the quantum-confined cadmium sulfide sluster: quenched photoluminescence and enhanced two-photon absorption. Journal of Physical Chemistry B 2006;110:19711–6;
(b) Wang XM, Zhou XY, Yu WT, Fang Q, et al. Two-photon pumped lasing stilbene-type chromophores containing various terminal donor groups: relationship between lasing efficiency and intramolecular charge transfer. Journal of Materials Chemistry 2000;10:2698–703.

[3] (a) Wang XM, Wang D, Zhou GY, et al. Symmetric and asymmetric charge transfer process of two-photon absorbing chromophores: bis-donor substituted stilbenes, and substituted styrylquinolinium and styrylpyridinium derivatives. Journal of Material Chemistry 2001;11:1600–5;
(b) Yan YL, Li B, Liu KJ, et al. Enhanced two-photon absorption and ultrafast dynamics of a new multibranched chromophore with a dibenzothiophene core. Journal of Physical Chemistry A 2007;111:4188–94.

[4] (a) Wang XM, Jin F, Chen ZG, et al. A new family of dendrimers with naphthaline core and triphenylamine branching as a two-photon polymerization initiator. Journal of Physical Chemistry C 2011;115:776–84;
(b) Wang XM, Jin F, Zhang WZ, et al. Novel $D-\pi_3-(A)_{1-3}$ multibranched chromophores as an efficient two-photon-induced polymerization initiator. Dyes and Pigments 2011;88:57–64.

[5] (a) Hu ZJ, Zhang RL, Sun PP, et al. Three asymmetrical conjugated $D-\pi-D'$ sulfur-containing chromophores with a focus on two-photon absorption. Australian Journal of Chemistry 2011;64:174–9;
(b) Abbotto A, Beverina L, Bradamante S, et al. Design and synthesis of heterocyclic multi-branched dyes for two-photon absorption. Synthetic Metals 2003;136:795–7;
(c) He GS, Lin T, Prasad PN. Toward highly active two-photon absorbing liquids. Synthesis and characterization of 1,3,5-triazine-based octupolar molecules. Chemistry of Materials 2004;16:185–94.

[6] Collini E. Cooperative effects to enhance two-photon absorption efficiency: inta- versus inter-molecular approach. Physical Chemistry Chemical Physics 2012;14:3725–36.

[7] (a) Fabbrini G, Menna E, Maggini M, Canazza A, Marcolongo G, Meneghetti M. Zinc-induced switching of the nonlinear optical properties of a functionalized bis(styryl)benzene. Journal of American Chemical Society 2004;126:6238–9;
(b) Kim HM, Jeong MY, Ahn HC, Jeon SJ, Cho BR. Two-photon sensor for metal ions derived from azacrown ether. Journal of Organic Chemistry 2004;69:5749–51;
(c) Righetto S, Rondena S, Locatelli D, Roberto D, Tessore F, Ugo R, et al. An investigation on the two-photon absorption activity of various terpyridines and related homoleptic and heteroleptic cationic Zn(II) complexes. Journal of Material Chemistry 2006;16:1439–44.

[8] Cheng LH, Li L, Sun PP, Zhou HP, et al. Synthesis, structure and nonlinear optical properties of two-photon absorption chromophores. Science in China Series B – Chemistry 2009;4:529–34.

[9] Reynolds GA, Drexhage KH. New coumarin dyes with rigidized structure for flashlamp-pumped dye lasers. Optics Communications 1975;13:222–5.

[10] Hu ZJ, Yang JX, Tian YP, Zhou HP, et al. Synthesis, structures, and optical properties of two novel two-photon initiators derived from 2,2′:6′2″- terpyridine. Bulletin of the Chemical Society of Japan 2007;80:986–93.

[11] Jin F, Zhou HP, Tian YP, et al. Synthesis, crystal structures, and optical properties of a novel imidazole derivative and its Zn(II) complex. Journal of Molecular Structure 2007;829:202–7.

[12] Mongin O, Porres L, Kahn C, Pons T, Mertz J, Blanchard-Desce M. Synthesis and two-photon absorption of highly soluble three-branched fluorenylene-vinylene derivatives. Tetrahedron Letters 2003;44:8121–5.

[13] (a) Hehre WJ, Ditchfield R, Pople JA. Molecular orbital theory of the electronic structure of organic compounds. V. molecular theory of bond separation. Journal of American Chemical Society 1970;92:4796–801;

(b) Hehre WJ, Ditchfield R, Pople JA. Self-consistent molecular orbital methods: XII. Further extentions of Gaussian-Type basis sets for use in molecular orbital studies of organic molecules. Journal of Chemical Physics 1972;56:2257–61.

[14] (a) Becke AD. Density-functional thermochemistry. III. The role of exact exchange. Journal of Chemical Physics 1993;98:5648–52;
(b) Becke AD. Density-functional exchange-energy approximation with correct asymptotic behavior. Physical Review A 1988;38:3098–100.

[15] (a) Bauernschmitt R, Ahlrichs R. Treatment of electronic excitations within the adiabatic approximation of time dependent density-functions theory. Chemical Physics Letters 1996;256:454–64;
(b) Casida ME, Jamorski C, Casida KC, Salahub DR. Molecular excitation energies to high-lying bound states from time-dependent density-functional response theory: characterizaton and correction of the time-dependent local density approximation ionization threshold. Journal of Chemical Physics 1998;108:4439–49.

[16] Frisch MJ, Trucks GW, Schlegel HB, et al. In: Gaussian 03, A.11. 4th ed. Pittsburgh, PA: Gaussian, Inc.; 2003.

[17] (a) Terenziani F, Katan C, Badaeva E, Tretiak S, Blanchard-Desce M. Enhanced two-photon absorption of organic chromophores: theoretical and experimental assessments. Advanced Materials 2008;20:4641–78;
(b) He GS, Tan LS, Zheng Q, Prasad PN. Multiphoton absorbing materials: molecular designs, characterizations, and applications. Chemical Reviews 2008;108:1245–330;
(c) Kim HM, Cho BR. Nonblinking and nonbleaching upconverting nanoparticles as an optical imaging nanoprobe and T_1 magnetic resonance imaging contract agent. Chemical Communications 2009;2:153–64;
(d) Pawlicki M, Collins HA, Denning RG, Anderson HL. Two-photon absorption and the design of two-photon dyes. Angewandte Chemie International Edition 2009;48:3244–66.

[18] (a) Kogej T, Beljonne D, Meyers F, et al. Mechanisms for enhancement of two-photon absorption in donor-acceptor conjugated chromophores. Chemical Physics Letters 1998;298:1–6;
(b) Wiirthner F, Archetti G, Schmidt R, Kuball HG. Solvent effect on color, band shape, and charge-density distribution for merocyanine dyes close to the cyanine limit. Angewandte Chemie International Edition 2008;47:4529–32.

[19] Zhou HP, Zhou FX, Wu P, et al. Three new five-coordinated mercury (II) dyes: structure and enhanced two-photon absorption. Dyes and Pigments 2011;91:237–47.

[20] Bublitz GU, Ortiz R, Marder SR, et al. Stark spectroscopy of donor–acceptor polyenes:correlation with nonlinear optical measurements. Journal of American Chemical Society 1997;119:2311–2.

[21] Xu C, Webb WW. Measurement of two-photon excitation cross sections of molecular fluorophores with data from 690 to 1050 nm. Journal of the Optical Society of America B 1997;13:481–91.

[22] Varnavski O, Goodson T, Sukhomlinova L, Twieg R. Ultrafast exciton dynamics in a branched molecule investigated by time-resolved fluorescence, transient absorption, and three-Pulse photon echo peak shift measurements. Journal of Physical Chemistry B 2004;108:10,484–10,492.

[23] Albota MA, Xu C, Webb WW. Two-photon fluorescence excitation cross sections of biomolecular probes from 690 to 960 nm. Applied Optics 1998;37:7352–6.

[24] Li ZG, Wu WB, Qin JG, et al. Dendronlike main-chain nonlinear optical (NLO) polyurethanes constructed from “H”-type chromophores: synthesis and NLO properties. Applied Materials & Interfaces 2009;4:856–63.